

RESEARCH LETTER

10.1002/2016GL069145

Key Points:

- S wave velocity decrease of ~0.02% after the 2003 San Simeon earthquake and ~0.2% after the 2004 Parkfield earthquake
- The minimum depth extent of velocity decrease is ~2.3 km for the San Simeon earthquake and ~1.2 km for the Parkfield earthquake
- Best explained by material damage and healing resulting mainly from dynamic stress perturbation of the two large earthquakes

Supporting Information:

- Figure S1
- Figure S2
- Figure S3
- Figure S4
- Supporting Information S1
- Figure S5

Correspondence to:

C. Wu,
cwu6@memphis.edu

Citation:

Wu, C., A. Delorey, F. Brenguier, C. Hadzioannou, E. G. Daub, and P. Johnson (2016), Constraining depth range of S wave velocity decrease after large earthquakes near Parkfield, California, *Geophys. Res. Lett.*, 43, 6129–6136, doi:10.1002/2016GL069145.

Received 13 APR 2016

Accepted 25 MAY 2016

Accepted article online 27 MAY 2016

Published online 20 JUN 2016

Constraining depth range of S wave velocity decrease after large earthquakes near Parkfield, California

Chunquan Wu¹, Andrew Delorey², Florent Brenguier³, Celine Hadzioannou⁴, Eric G Daub¹, and Paul Johnson²

¹Center of Earthquake Research and Information, University of Memphis, Memphis, Tennessee, USA, ²Geophysics Group, Los Alamos National Laboratory, Los Alamos, New Mexico, USA, ³Institut des Sciences de la Terre, Grenoble, France,

⁴Department of Earth and Environmental Sciences, Ludwig Maximilians University, Munich, Germany

Abstract We use noise correlation and surface wave inversion to measure the S wave velocity changes at different depths near Parkfield, California, after the 2003 San Simeon and 2004 Parkfield earthquakes. We process continuous seismic recordings from 13 stations to obtain the noise cross-correlation functions and measure the Rayleigh wave phase velocity changes over six frequency bands. We then invert the Rayleigh wave phase velocity changes using a series of sensitivity kernels to obtain the S wave velocity changes at different depths. Our results indicate that the S wave velocity decreases caused by the San Simeon earthquake are relatively small (~0.02%) and access depths of at least 2.3 km. The S wave velocity decreases caused by the Parkfield earthquake are larger (~0.2%), and access depths of at least 1.2 km. Our observations can be best explained by material damage and healing resulting mainly from the dynamic stress perturbations of the two large earthquakes.

1. Introduction

Cross correlation of ambient seismic noise has been shown to efficiently reconstruct empirical Green's function between a pair of seismic stations [e.g., Lobkis and Weaver, 2001]. As recording ambient seismic noise is less expensive than active source experiments, and provides better temporal coverage than natural repeating earthquakes, many recent studies have used ambient noise cross correlation to monitor temporal changes in seismic velocity in the crust. These studies observed velocity changes caused by nearby large earthquakes [Brenguier et al., 2008a; Wegler et al., 2009; Chen et al., 2010; Zhao et al., 2010; Zaccarelli et al., 2011; Hobiger et al., 2012; Schaff, 2012; Takagi et al., 2012; Lesage et al., 2014; Liu et al., 2014], volcanic activities [Brenguier et al., 2008b; Brenguier et al., 2014], aseismic slow slip events [Rivet et al., 2011], and seasonal variations [Sens-Schonfelder and Wegler, 2006; Meier et al., 2010].

After the 2003 *M*6.5 San Simeon earthquake and the 2004 *M*6.0 Parkfield, temporal changes in the seismic velocity in the Parkfield region are documented by previous studies using natural repeating earthquakes [Rubinstein and Beroza, 2005], active sources [Li et al., 2006, 2007], and ambient noise cross correlation [Brenguier et al., 2008a]. However, the observations from these studies do not put quantitative constraints on the depth extent of the velocity changes, which is crucial for the interpretation of the results and determination of the underlying physical mechanisms of the seismic velocity changes.

Here we apply seismic noise correlation to continuous recordings near Parkfield over six different frequency ranges and use surface wave inversion to infer the S wave velocity changes at different depths after the San Simeon and the Parkfield earthquakes. We then compare our results with those from previous studies, and finally, we discuss some possible explanations and implications of the observations.

2. Data and Analysis Procedure

We use continuous seismic recordings at 13 High Resolution Seismic Network (HRSN) stations in the vicinity of the Parkfield region (Figure 1). We select these borehole stations at depths of 60–150 m to diminish potential incoherent noise from the surface of the earth. We analyze data from May 2001 to April 2011, including the records of two nearby major earthquakes: the 2003 *M*6.5 San Simeon earthquake and the 2004 *M*6.0 Parkfield earthquake.

The analysis procedure in this study generally follows those in Brenguier et al. [2008a] and Lecocq et al. [2014] and is briefly described here. We first download the continuous recordings from the Northern California

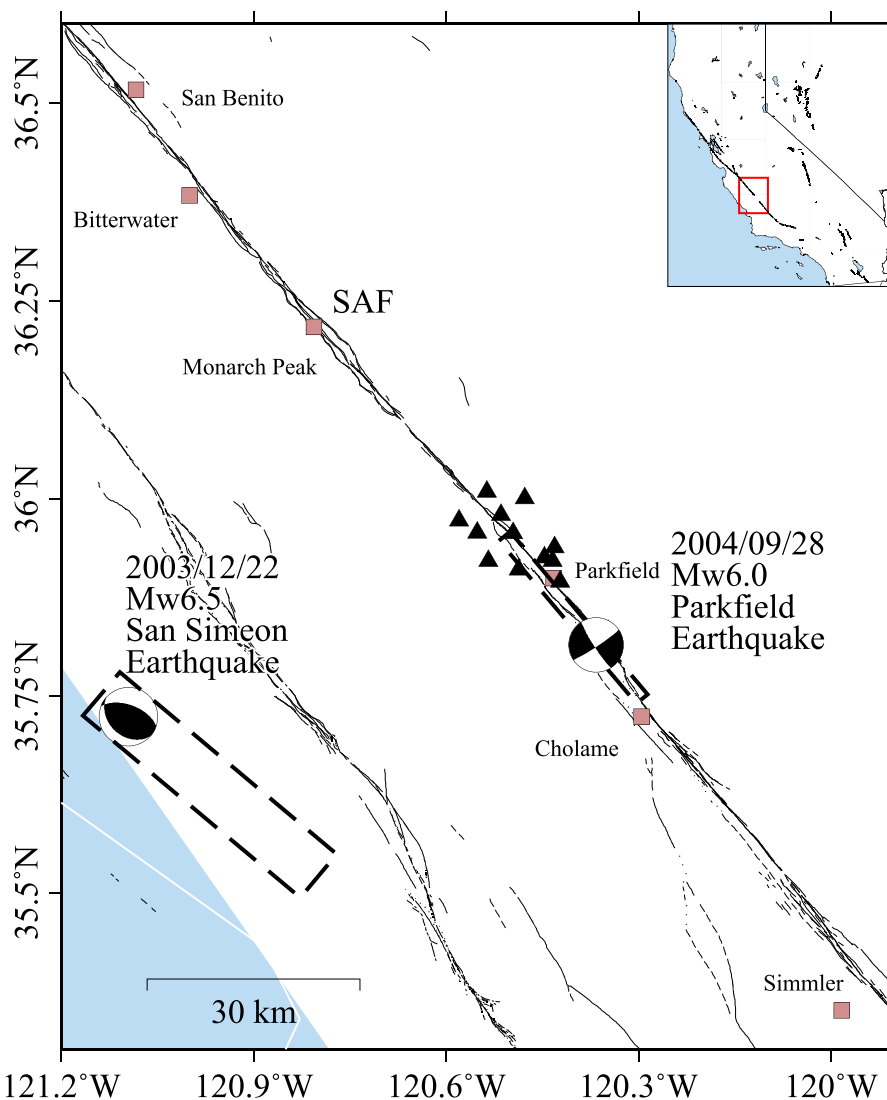


Figure 1. (a) Map of the study region of central California. The black triangles show the locations of the HRSN stations. The epicenters of the 2003 M_w 6.5 San Simeon and the 2004 M_w 6.0 Parkfield earthquakes are indicated by the moment tensor solution, with the black dashed boxes showing the rupture zones [Chen et al., 2004; Bennington et al., 2011]. The black lines indicate active faults, and the brown squares indicate nearby geographical locations. The inset is a map of California with the red box showing the region plotted in the main map.

Earthquake Data Center (www.ncedc.org), and then we organize the continuous recordings into 1 day segments, resampling all the data to 20 Hz. Then we use the MSNoise package [Lecocq et al., 2014] for computing the noise cross correlation. We first scan all the data into a MySQL database, define different frequency ranges (0.2–0.6 Hz, 0.3–0.8 Hz, 0.5–1.0 Hz, 0.7–1.2 Hz, 0.9–1.4 Hz, and 1.2–2.0 Hz) based on the frequency range of ambient seismic noise and the instrument response range of the HRSN stations and then create cross-correlation jobs of different station pairs. For each station pair, the vertical component recordings are clipped to three times the root-mean-square (RMS) value and then whitened within the predefined frequency ranges. The cross correlations between all the station pairs are then computed and stacked for every 30 days. An example of the stacked cross-correlation functions (CCFs) from a station pair CCRB-EADB at frequency range 0.5–1.0 Hz is shown in Figure 2. We also checked the stacked CCFs at different frequency ranges (e.g., Figure S1 in the supporting information) and for different station pairs (e.g., Figure S2) to ensure that the CCFs are dominated by Rayleigh waves. After the computation and stack of CCFs are completed, we use the stacked CCFs from vertical components as empirical Green's functions for Rayleigh wave propagation between a pair of stations [Shapiro and Campillo, 2004], and we average all the

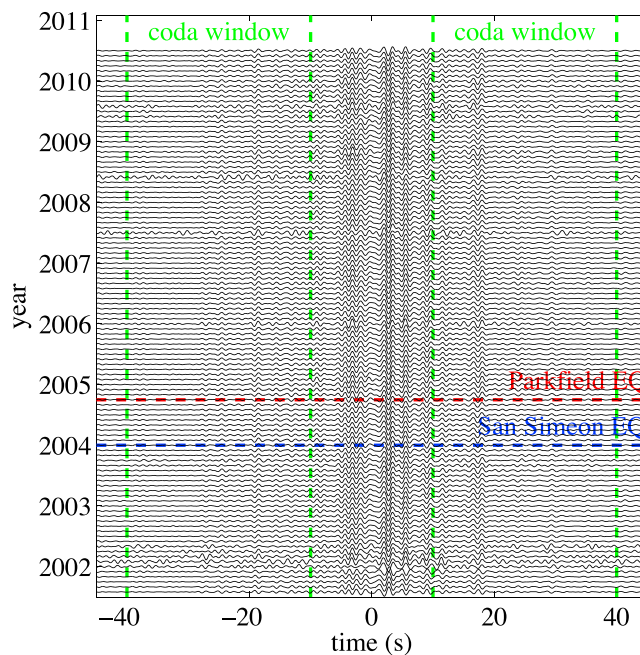


Figure 2. Example of 30 day stacked cross-correlation functions (CCFs) for the station pair CCRB-EADB from 2001 to 2010. The CCFs are computed using the vertical component of the recordings filtered at the frequency band 0.5–1.0 Hz. The vertical green dashed lines mark the coda windows from –40 to –10 s and from 10 to 40 s. The horizontal blue and red dashed lines mark the timings of the San Simeon and the Parkfield earthquake, respectively.

velocity [Delorey et al., 2007]. We use a starting velocity model for Parkfield retrieved from the Southern California Earthquake Center (SCEC, doi:10.7909/C3WD3xH1) community velocity model (Figure S3) and calculate Rayleigh wave phase velocities at center frequencies of the six frequency ranges: 0.40, 0.55, 0.75, 0.95, 1.15, and 1.6 Hz. Then we convert the observed time delays from CCFs to Rayleigh wave phase velocity changes by assuming that the phase velocity changes are proportional to the observed time delays (i.e., $dt/t = -dC/C$) and use them to perturb the Rayleigh wave phase velocities calculated from the SCEC community velocity model according to changes in Rayleigh wave phase velocities. With these perturbed Rayleigh wave phase velocities, we invert for a 1-D S wave velocity model using a series of sensitivity kernels (Figure S4) and compare to the starting model to obtain the S wave velocity changes. Since the inversion results are highly nonunique, we use two different normalizations in our inversion to constrain the depth range of the velocity changes. First, we apply damping that is uniform with depth. This is the “unsqueezed” solution. Then we apply progressively higher levels of damping starting with the deepest part of the model and progressively moving upward. When the final model misfit exceeds the misfit of the unsqueezed solution, we stop and select the last solution whose misfit is the same or better than the unsqueezed model. This is the “squeezed” solution. In this way we can estimate the minimum depths in which velocities changes have occurred.

3. Results

After applying the noise cross-correlation algorithm to each station pair, we generate ~3200 days of stacked CCFs for each of the six frequency ranges. Each stacked CCF is averaged from 30 consecutive daily CCFs (e.g., Figure 2). The measured relative time delays averaged from all stations pairs are shown in Figure 3, and the measured peak time delays immediately after the San Simeon and the Parkfield earthquakes are shown in Table 1 and Figure 4. We observe smaller relative time delays (~0.02–0.05%) in the Rayleigh wave coda for all the six frequency ranges after the San Simeon earthquake, and larger relative time delays (~0.05–0.2%) after the Parkfield earthquake. For the San Simeon earthquake, the relative time delays do not vary significantly for the six different frequency ranges. However, for the Parkfield earthquake, the relative time delays

stacked CCFs to obtain a reference CCF. We use a moving-window cross-spectral method to measure the relative dephasing between the 30 day stacks of CCFs and the reference CCF, and then obtain the time delays for all the station pairs and frequency ranges [Clarke et al., 2011]. We use the coda (10–40 s before and after the zero time, see Figure S1) instead of the direct arrival (0–10 s before and after the zero time) of the CCFs to measure the time delay, as the multiple deflected waves sample the medium better than the direct arrival waves [Snieder, 2004]. The overall time delay is then obtained by averaging time delays from all the station pairs using a weighted averaging method based on the uncertainty from each station pair [Lecocq et al., 2014].

In order to determine changes in S wave velocity as a function of depth from the changes in Rayleigh wave phase velocity as a function of frequency, we use the forward model of Takeuchi and Saito [1972] and iteratively invert for changes in shear wave

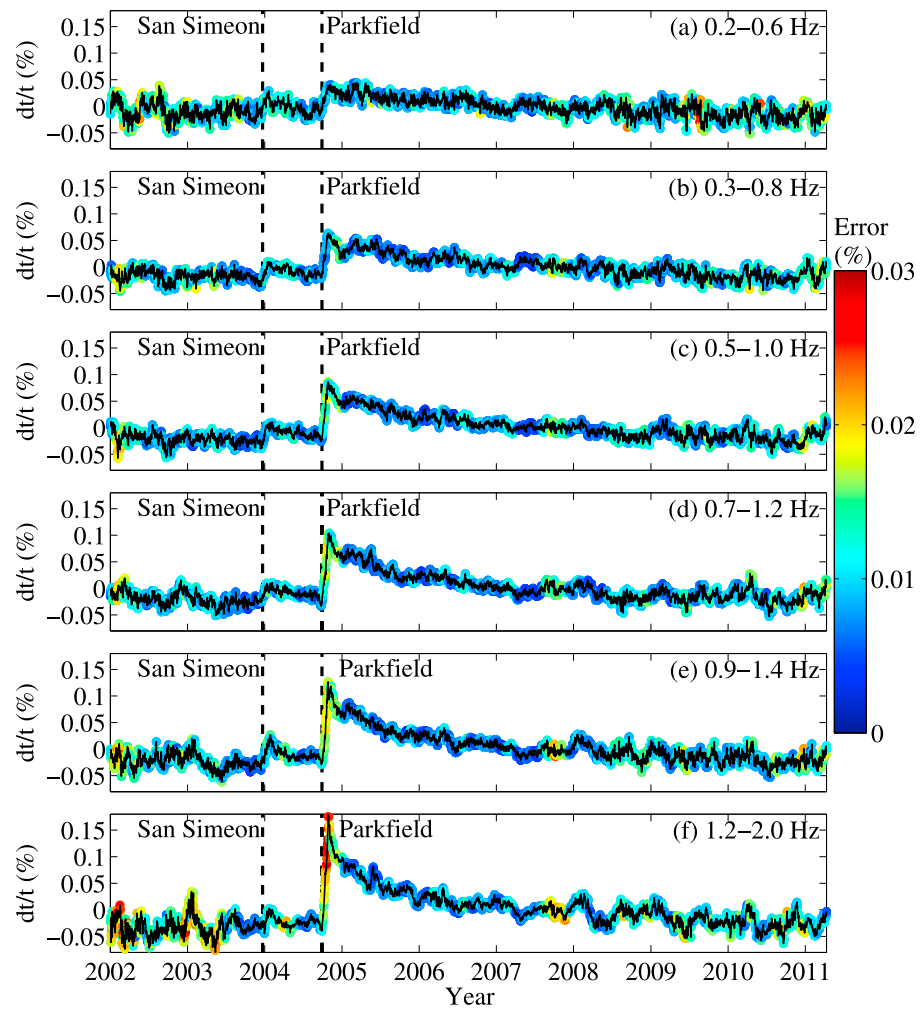


Figure 3. Measured percentage time delays (black curve) from the stacked CCFs for the six frequency bands. The X axis is the calendar year, and the Y axis is the time delay in percentage. The color shows uncertainties at each data point. The two vertical dashed lines indicate the timings of the 2003 San Simeon and the 2004 Parkfield earthquakes.

for higher-frequency ranges are significantly larger than those for lower frequency ranges (Figure 4). After the Parkfield earthquake, the relative time delays gradually decrease to the background level in ~3 years for all the six frequency ranges (Figure 3).

The inversion results suggest decreases in S wave velocities at different depths after the San Simeon and the Parkfield earthquakes, with generally larger decreases at shallower depths (Figure 5). For the San Simeon earthquake, the unsqueezed inversion results suggest that the S wave velocity drop extends to ~7 km and the largest drop is ~0.02% at the depth of 2.5 km. One the other hand, the squeezed inversion results suggest that the depth

Table 1. Measured Time Delays in Percentage and Uncertainties for the Six Frequency Ranges After the 2003 San Simeon and the 2004 Parkfield Earthquakes

Frequency (Hz)	San Simeon Earthquake		Parkfield Earthquake	
	dt/t (%)	Uncertainty (%)	dt/t (%)	Uncertainty (%)
0.2–0.6	0.0381	0.0093	0.0482	0.0087
0.3–0.8	0.0260	0.0106	0.0798	0.0100
0.5–1.0	0.0304	0.0102	0.1067	0.0173
0.7–1.2	0.0302	0.0117	0.1232	0.0127
0.9–1.4	0.0489	0.0155	0.1485	0.0172
1.2–2.0	0.0348	0.0106	0.2138	0.0245

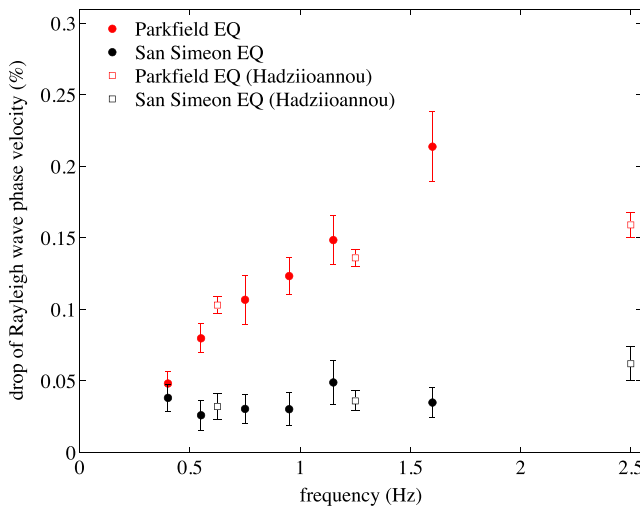


Figure 4. Percentage drop of Rayleigh wave phase velocity plotted again frequency after the San Simeon (black circles) and the Parkfield (red circles) earthquakes. The vertical bars show the uncertainty associated with each measurement. The results from Hadzioannou et al. are shown in black and red open squares for comparison.

different approaches. Specifically, *Rubinstein and Beroza [2005]* examined two sequences of repeating earthquakes and found much larger time delays from *S* wave recorded by surface stations than that from borehole stations after the Parkfield earthquake and suggested that the velocity drop is likely to be limited to the top 100 m. *Li et al. [2006, 2007]* investigated *S* wave velocity changes after the Parkfield earthquake using active

of *S* wave velocity drop need to be at least 2.3 km to generate the observed time delays from Rayleigh wave coda. For the Parkfield earthquake, the unsqueezed inversion results suggest *S* wave velocity drop in the top 5 km with the largest drop is ~0.2% in the top 1 km, and the squeezed inversion results suggest that *S* wave velocity drop need to be at least 1.2 km in depth to generate the observed time delays from Rayleigh wave coda.

4. Discussion

In this study, we find *S* wave velocity decreases at different depths from the observed time delays in CCFs reconstructed by noise correlation. Previous studies have observed seismic wave velocity decrease after the 2004 Parkfield earthquake from

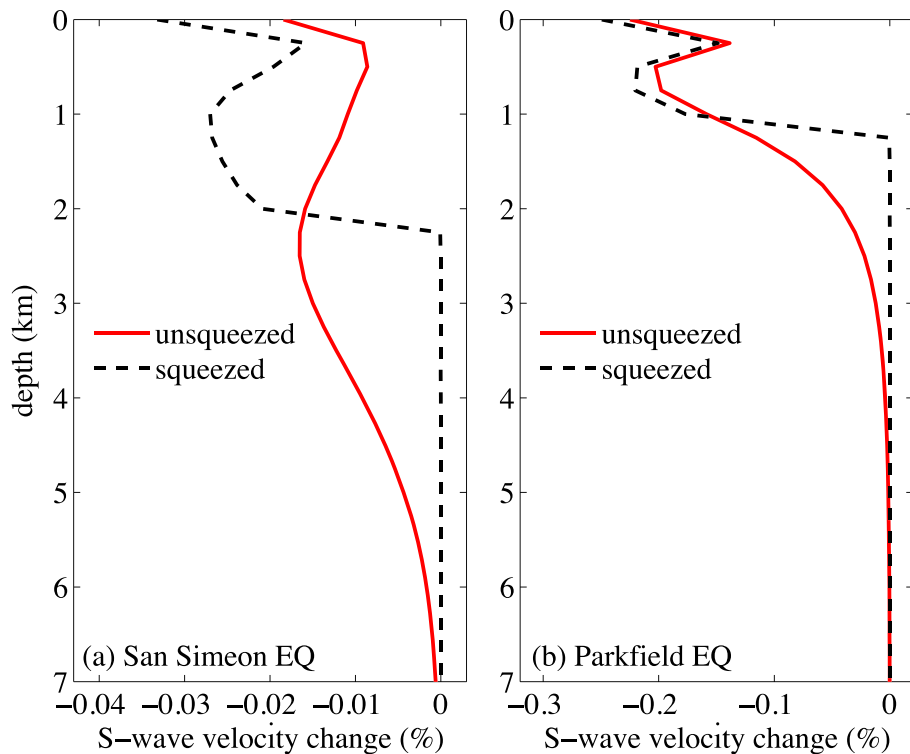


Figure 5. Inverted *S* wave velocity changes in percentage at difference depths. The red solid curve shows the unsqueezed solution, and the black dashed curve shows the squeezed solution for (a) the San Simeon earthquake and (b) the Parkfield earthquake.

sources. They found a 0.2%–0.5% S wave velocity decrease outside the fault zone after the Parkfield earthquake, which is comparable to our results (Figure 5). However, due to the episodic nature of natural repeating earthquake sequences and high cost of active source experiments, it is not possible to monitor the seismic velocity changes continuously and measure the velocity decrease immediately after the Parkfield earthquake using these approaches. *Brenguier et al.* [2008a] applied the noise correlation approach to the HRSN continuous data from 2002 to 2007, and they observed Rayleigh wave phase velocity decrease of ~0.02% after the San Simeon earthquake and ~0.06% after the Parkfield earthquake followed by gradual recovery. Hadzioannou et al. analyzed the same data set as *Brenguier et al.* [2008a] with all three components and three frequency bands. They found that the velocity drops after the San Simeon and Parkfield earthquake are frequency dependent (Figure 4) and the materials at different sides of the San Andreas fault show different velocity drops and recovery rates (Celine Hadzioannou, personal communication, 2015). Here we extend the analysis of *Brenguier et al.* [2008a] to six different frequency ranges with a longer time period from 2001 to 2011. We observe a similar decrease and recovery of Rayleigh wave phase velocity as *Brenguier et al.* [2008a] in all the six frequency ranges (Figure 3). Our additional analysis provides a method to constrain the depth range of the physical processes responsible for the velocity changes.

The observed drop in seismic velocity after large earthquakes and the following recovery have been commonly attributed to material damage and healing process [e.g., *Rubinstein and Beroza*, 2005; *Li et al.*, 2007; *Brenguier et al.*, 2008a; *Wu et al.*, 2009; *Lesage et al.*, 2014]. In these cases, the mechanism of material damage is argued to be either crack opening or reduced packing within weak sedimentary layers and fault zones [Marone, 1998]. This mechanism is also observed in laboratory experiments with granular material and rocks [Guyer and Johnson, 1999; Johnson and Jia, 2005; Johnson and Sutin, 2005], small-scale field experiments [Johnson et al., 2009; Renaud et al., 2014], and simulated with damage rheology models [Lyakhovsky and Ben-Zion, 2008; Finzi et al., 2009]. The laboratory and small field experiments also observed gradual logarithmic time recovery of velocity, also termed as “slow dynamics” [Johnson and Sutin, 2005; Johnson et al., 2009], which is consistent with the gradual recovery of seismic velocities observed in this study (Figure 3) and previous studies [e.g., Schaff and Beroza, 2004; Rubinstein and Beroza, 2005]. Another possible mechanism is increase of water flow after large earthquakes [Brodsky et al., 2003; Elkhouri et al., 2006; Manga and Wang, 2007], which suggests that large earthquakes could increase the permeability of the crust, resulting in an increase in porosity and decrease in S wave velocity. However, this mechanism requires significant presence of fluids in the crust, and it is often related to hydrological and volcanic regions. There is no evidence of large fluid presence in our study region, and in addition, this mechanism could not explain the observation of generally larger S wave velocity decrease at shallower depths (Figure 5), so change of fluid flow is not likely to be the major cause of the depth pattern of the observed S wave velocity changes. Hence, our results suggest that the material damage and healing mechanism is the dominant mechanism.

The inversion results in this study indicate that the depth extent of S wave velocity decrease caused by the San Simeon earthquake is at least 2.3 km and the depth range of S wave velocity decrease caused by the Parkfield earthquake is at least 1.2 km. The validity of the inversion results is based on the assumption that the coda part of CCF is dominated by surface waves energy. Previous studies have shown that the early part of coda is dominated by surface waves energy, while body waves energy could contribute to the later part of the coda [Obermann et al., 2013]. However, we found clear frequency dependency of the velocity decrease after the two earthquakes (Figures 3 and 4), suggesting that the frequency-dependent portion of the velocity decrease is likely due to surface waves dispersion, as body waves sensitivity originates from the scattering process, which could result in both velocity increase and decrease [Stein and Wysession, 2003]. Recently, *Lesage et al.* [2014] use a similar approach as this study to investigate the S wave velocity changes in the region of Colima Volcano, Mexico, after the 2003 $M7.4$ Tecoman earthquake. Through inversion, they found S wave velocity decrease in the top ~1 km. If the observed S wave velocity decreases are caused by material damage, these recent studies suggest that the material damage from nearby large earthquakes is probably not limited to very shallow sediments [Rubinstein and Beroza, 2005], although the damage to the less confined shallow sediments is likely to be much larger than the damage to the deeper part [Li et al., 2007]. Indeed, laboratory studies have found that the shear modulus of rocks and unconsolidated granular materials decreases at dynamic wave strain amplitude of 10^{-6} or higher [Johnson and Jia, 2005; Johnson and Sutin, 2005]. According to strong ground records at the surface, the peak ground accelerations are 0.15 g for the San Simeon earthquake and >2.5 g for the Parkfield earthquake [Hardebeck et al., 2004; Bakun et al., 2005]. These values roughly correspond to peak ground

velocities of 0.16 m/s for the San Simeon earthquake and >1 m/s for the Parkfield earthquake [Wald *et al.*, 1999]. Using an S wave velocity of 2.7 km/s at the surface from the SCEC community velocity model (Figure S3), we could estimate the dynamic strains to be $\sim 5.9 \times 10^{-5}$ for the San Simeon earthquake and $>3.7 \times 10^{-4}$ for the Parkfield earthquake. These values are 1–2 magnitudes larger than the strain amplitude threshold of 10^{-6} . The dynamic strain at depth cannot be directly measured since there is no deep borehole seismic station at the depth of several kilometers near the Parkfield region during both large earthquakes, but they are probably well above the threshold of 10^{-6} due to the large values at the surface. On the other hand, some previous studies have suggested that static stress changes could also cause velocity changes by opening and closing existing cracks [Ratdomopurbo and Poupinet, 1995; Nishimura *et al.*, 2005; Chen *et al.*, 2010; Rivet *et al.*, 2011]. However, this mechanism could cause both velocity decrease and increase at different sites, which is not observed in our case. According to static stress modeling results, the positive static shear stresses at the top few kilometers in our study region are ~ 5 kPa for the San Simeon earthquake and ~ 15 kPa for the Parkfield earthquake [e.g., Shelly and Johnson, 2011]. These values correspond to static strains of $\sim 1.7 \times 10^{-7}$ for the San Simeon earthquake and $\sim 5.0 \times 10^{-7}$ for the Parkfield earthquake, assuming a typical shear rigidity value of 30 GPa for sedimentary rocks. The estimated static strains are much smaller than the estimated dynamic strains, so the contribution to material damage from the static strains are not likely to be as significant as that from the dynamic strains. In addition, we observe much weaker frequency dependence of time delays for the San Simeon earthquake than that for the Parkfield earthquake (Figure 4). As the San Simeon earthquake is further away (~ 60 km) from our study region, the energy in the seismic waves attenuates more than that from the Parkfield earthquake, resulting in much weaker dynamic stress perturbations in the higher-frequency ranges compared to those from the Parkfield earthquake.

5. Conclusion

We apply noise correlation and surface wave inversion to ~ 10 years of continuous seismic recordings at the HRSN network in Parkfield, California. We find an S wave velocity decrease of $\sim 0.02\%$ after the 2003 San Simeon earthquake and an S wave velocity decrease of $\sim 0.2\%$ after the 2004 Parkfield earthquake followed by gradual recovery of ~ 3 years. The minimum depth extent of velocity decrease we estimate is ~ 2.3 km for the San Simeon earthquake and ~ 1.2 km for the Parkfield earthquake. Our observations are best explained by the mechanism of material damage and healing resulting mainly from dynamic stress perturbation of the two large earthquakes, and suggest that the material damage occurred over depth ranges of at least several kilometers. This study, together with other recent studies [e.g., Rivet *et al.*, 2011; Lesage *et al.*, 2014; Obermann *et al.*, 2014], suggests that noise correlation combined with surface wave inversion is an effective new approach to monitor continuous time evolution of seismic velocity changes at different depths of the crust and the velocity changes at different depths could be governed by different mechanisms.

Acknowledgments

This research was supported by Institutional Support at Los Alamos National Lab (C.W., A.D., and P.J.), ISTerre (F.B.), CERI (C.W. and E.G.D.), and the Emmy Noether program (HA 7019/1-1) of the German Research Foundation (C.H.). We thank Thomas Lecocq and Corentin Caudron for providing the MSnoise package (www.msnoise.org). We thank Joan Gomberg and Robert Guyer for helpful discussions. All the seismic data are obtained from the Northern California Earthquake Data Center (NCEDC) website (www.ncedc.org).

References

- Bakun, W., B. Aagaard, B. Dost, W. Ellsworth, J. Hardebeck, R. Harris, C. Ji, M. Johnston, J. Langbein, and J. Lienkaemper (2005), Implications for prediction and hazard assessment from the 2004 Parkfield earthquake, *Nature*, 437(7061), 969–974.
- Bennington, N., C. Thurber, K. L. Feigl, and J. Murray-Moraleda (2011), Aftershock distribution as a constraint on the geodetic model of coseismic slip for the 2004 Parkfield earthquake, *Pure Appl. Geophys.*, 168(10), 1553–1565.
- Brenguier, F., M. Campillo, C. Hadzioannou, N. Shapiro, R. Nadeau, and E. Larose (2008a), Postseismic relaxation along the San Andreas fault at Parkfield from continuous seismological observations, *Science*, 321(5895), 1478.
- Brenguier, F., N. M. Shapiro, M. Campillo, V. Ferrazzini, Z. Duputel, O. Coutant, and A. Nercessian (2008b), Towards forecasting volcanic eruptions using seismic noise, *Nat. Geosci.*, 1(2), 126–130.
- Brenguier, F., M. Campillo, T. Takeda, Y. Aoki, N. Shapiro, X. Briand, K. Emoto, and H. Miyake (2014), Mapping pressurized volcanic fluids from induced crustal seismic velocity drops, *Science*, 345(6192), 80–82.
- Brodsky, E., E. Roeloffs, D. Woodcock, I. Gall, and M. Manga (2003), A mechanism for sustained groundwater pressure changes induced by distant earthquakes, *J. Geophys. Res.*, 108(B8), 2390, doi:10.1029/2002JB002321.
- Chen, J. H., B. Froment, Q. Y. Liu, and M. Campillo (2010), Distribution of seismic wave speed changes associated with the 12 May 2008 $M_w 7.9$ Wenchuan earthquake, *Geophys. Res. Lett.*, 37, L18302, doi:10.1029/2010GL044582.
- Chen, J., K. M. Larson, Y. Tan, K. W. Hudnut, and K. Choi (2004), Slip history of the 2003 San Simeon earthquake constrained by combining 1-Hz GPS, strong motion, and teleseismic data, *Geophys. Res. Lett.*, 31, L17608, doi:10.1029/2004GL020448.
- Clarke, D., L. Zaccarelli, N. Shapiro, and F. Brenguier (2011), Assessment of resolution and accuracy of the Moving Window Cross Spectral technique for monitoring crustal temporal variations using ambient seismic noise, *Geophys. J. Int.*, 186(2), 867–882.
- Delaney, A. A., R. A. Dunn, and J. B. Gaherty (2007), Surface wave tomography of the upper mantle beneath the Reykjanes Ridge with implications for ridge–hot spot interaction, *J. Geophys. Res.*, 112, B08313, doi:10.1029/2006JB004785.
- Elkhouri, J., E. Brodsky, and D. Agnew (2006), Seismic waves increase permeability, *Nature*, 441(7097), 1135–1138.

- Finzi, Y., E. Hearn, Y. Ben-Zion, and V. Lyakhovsky (2009), Structural properties and deformation patterns of evolving strike-slip faults: Numerical simulations incorporating damage rheology, *Pure Appl. Geophys.*, **166**, 1537–1573.
- Guyer, R. A., and P. A. Johnson (1999), Nonlinear mesoscopic elasticity: Evidence for a new class of materials, *Phys. Today*, **52**(4), 30–36.
- Hardebeck, J. L., J. Boatwright, D. Dreger, R. Goel, V. Graizer, K. Hudnut, C. Ji, L. Jones, J. Langbein, and J. Lin (2004), Preliminary report on the 22 December 2003, M 6.5 San Simeon, California earthquake, *Seismol. Res. Lett.*, **75**(2), 155–172.
- Hobiger, M., U. Wegler, K. Shiomi, and H. Nakahara (2012), Coseismic and postseismic elastic wave velocity variations caused by the 2008 Iwate-Miyagi Nairiku earthquake, Japan, *J. Geophys. Res.*, **117**, B09313, doi:10.1029/2012JB009402.
- Johnson, P., and A. Sutin (2005), Slow dynamics and anomalous nonlinear fast dynamics in diverse solids, *J. Acoustic. Soc. Am.*, **117**(1), 124–130.
- Johnson, P. A., P. Bodin, J. Gomberg, F. Pearce, Z. Lawrence, and F. Y. Menq (2009), Inducing *in situ*, nonlinear soil response applying an active source, *J. Geophys. Res.*, **114**, B05304, doi:10.1029/2008JB005832.
- Johnson, P., and X. Jia (2005), Nonlinear dynamics, granular media and dynamic earthquake triggering, *Nature*, **437**, 871–874, doi:10.1038/nature04015.
- Lecocq, T., C. Caudron, and F. Brenguier (2014), MSNoise, a Python package for monitoring seismic velocity changes using ambient seismic noise, *Seismol. Res. Lett.*, **85**(3), 715–726.
- Lesage, P., G. Reyes-Dávila, and R. Arámbula-Mendoza (2014), Large tectonic earthquakes induce sharp temporary decreases in seismic velocity in Volcán de Colima, Mexico, *J. Geophys. Res. Solid Earth*, **119**, 4360–4376, doi:10.1002/2013JB010884.
- Li, Y., P. Chen, E. S. Cochran, J. E. Vidale, and T. Burdette (2006), Seismic evidence for rock damage and healing on the San Andreas fault associated with the 2004 M 6.0 Parkfield earthquake, *Bull. Seismol. Soc. Am.*, **96**(4B), S349–S363.
- Li, Y., P. Chen, E. Cochran, and J. Vidale (2007), Seismic velocity variations on the San Andreas fault caused by the 2004 M6 Parkfield Earthquake and their implications, *Earth Planets Space*, **59**(1), 21.
- Liu, Z., J. Huang, Z. Peng, and J. Su (2014), Seismic velocity changes in the epicentral region of the 2008 Wenchuan earthquake measured from three-component ambient noise correlation techniques, *Geophys. Res. Lett.*, **41**, 37–42, doi:10.1002/2013GL058682.
- Lobkis, O. I., and R. L. Weaver (2001), On the emergence of the Green's function in the correlations of a diffuse field, *J. Acoustic. Soc. Am.*, **110**(6), 3011–3017.
- Lyakhovsky, V., and Y. Ben-Zion (2008), Scaling relations of earthquakes and aseismic deformation in a damage rheology model, *Geophys. J. Int.*, **172**(2), 651–662.
- Manga, M., and C. Wang (2007), Earthquake hydrology, *Treatise Geophys.*, **4**, 293–320.
- Marone, C. (1998), Laboratory-derived friction laws and their application to seismic faulting, *Annu. Rev. Earth Planet. Sci.*, **26**(1), 643–696.
- Meier, U., N. M. Shapiro, and F. Brenguier (2010), Detecting seasonal variations in seismic velocities within Los Angeles basin from correlations of ambient seismic noise, *Geophys. J. Int.*, **181**(2), 985–996.
- Nishimura, T., S. Tanaka, T. Yamamoto, H. Yamamoto, T. Sano, H. Nakahara, N. Uchida, S. Hori, and H. Sato (2005), Temporal changes in seismic velocity of the crust around Iwate volcano, Japan, as inferred from analyses of repeated active seismic experiment data from 1998 to 2003, *Earth Planets Space*, **57**(6), 491–505.
- Obermann, A., T. Planès, E. Larose, C. Sens-Schönfelder, and M. Campillo (2013), Depth sensitivity of seismic coda waves to velocity perturbations in an elastic heterogeneous medium, *Geophys. J. Int.*, **194**(1), 372–382.
- Obermann, A., B. Froment, M. Campillo, E. Larose, T. Planès, B. Valette, J. Chen, and Q. Liu (2014), Seismic noise correlations to image structural and mechanical changes associated with the M_w 7.9 2008 Wenchuan earthquake, *J. Geophys. Res. Solid Earth*, **119**, 3155–3168, doi:10.1002/2013JB010932.
- Ratdomopurbo, A., and G. Poupinet (1995), Monitoring a temporal change of seismic velocity in a volcano: Application to the 1992 eruption of Mt. Merapi (Indonesia), *Geophys. Res. Lett.*, **22**(7), 775–778, doi:10.1029/95GL00302.
- Renaud, G., J. Rivière, C. Larmat, J. Rutledge, R. Lee, R. Guyer, K. Stokoe, and P. Johnson (2014), In situ characterization of shallow elastic nonlinear parameters with dynamic acoustoelastic testing, *J. Geophys. Res. Solid Earth*, **119**, 6907–6923, doi:10.1002/2013JB010625.
- Rivet, D., M. Campillo, N. M. Shapiro, V. Cruz-Atienza, M. Radiguet, N. Cotte, and V. Kostoglodov (2011), Seismic evidence of nonlinear crustal deformation during a large slow slip event in Mexico, *Geophys. Res. Lett.*, **38**, L08308, doi:10.1029/2011GL047151.
- Rubinstein, J., and G. Beroza (2005), Depth constraints on nonlinear strong ground motion from the 2004 Parkfield earthquake, *Geophys. Res. Lett.*, **32**, L14313, doi:10.1029/2005GL023189.
- Schaaff, D., and G. Beroza (2004), Coseismic and postseismic velocity changes measured by repeating earthquakes, *J. Geophys. Res.*, **109**, B10302, doi:10.1029/2004JB003011.
- Schaaff, D. P. (2012), Placing an upper bound on preseismic velocity changes measured by ambient noise monitoring for the 2004 M_w 6.0 Parkfield earthquake (California), *Bull. Seismol. Soc. Am.*, **102**(4), 1400–1416.
- Sens-Schönfelder, C., and U. Wegler (2006), Passive image interferometry and seasonal variations of seismic velocities at Merapi Volcano, Indonesia, *Geophys. Res. Lett.*, **33**, L21302, doi:10.1029/2006GL027797.
- Shapiro, N. M., and M. Campillo (2004), Emergence of broadband Rayleigh waves from correlations of the ambient seismic noise, *Geophys. Res. Lett.*, **31**, L07614, doi:10.1029/2004GL019491.
- Shelly, D. R., and K. M. Johnson (2011), Tremor reveals stress shadowing, deep postseismic creep, and depth-dependent slip recurrence on the lower-crustal San Andreas fault near Parkfield, *Geophys. Res. Lett.*, **38**, L13312, doi:10.1029/2011GL047863.
- Snieder, R. (2004), Extracting the Green's function from the correlation of coda waves: A derivation based on stationary phase, *Phys. Rev. E*, **69**(4), 046,610.
- Stein, S., and M. Wysession (2003), *An Introduction to Seismology, Earthquakes, and Earth Structure*, Blackwell, Malden, Mass.
- Takagi, R., T. Okada, H. Nakahara, N. Umino, and A. Hasegawa (2012), Coseismic velocity change in and around the focal region of the 2008 Iwate-Miyagi Nairiku earthquake, *J. Geophys. Res.*, **117**, B06315, doi:10.1029/2012JB009252.
- Takeuchi, H., and M. Saito (1972), Seismic surface waves, in *Methods in Computational Physics*, vol. 11, edited by B. A. Bolt, pp. 195–217, Academic Press, New York.
- Wald, D. J., V. Quitoriano, T. H. Heaton, and H. Kanamori (1999), Relationships between peak ground acceleration, peak ground velocity, and modified Mercalli intensity in California, *Earthq. Spectra*, **15**(3), 557–564.
- Wegler, U., H. Nakahara, C. Sens-Schönfelder, M. Korn, and K. Shiomi (2009), Sudden drop of seismic velocity after the 2004 M_w 6.6 mid-Niigata earthquake, Japan, observed with Passive Image Interferometry, *J. Geophys. Res.*, **114**, B06305, doi:10.1029/2008JB005869.
- Wu, C., Z. Peng, and D. Assimaki (2009), Temporal changes in site response associated with strong ground motion of 2004 M_w 6.6 mid-Niigata earthquake sequences in Japan, *Bull. Seismol. Soc. Am.*, **99**(6), 3487–3495.
- Zaccarelli, L., N. Shapiro, L. Faenza, G. Soldati, and A. Michelini (2011), Variations of crustal elastic properties during the 2009 L'Aquila earthquake inferred from cross-correlations of ambient seismic noise, *Geophys. Res. Lett.*, **38**, L24304, doi:10.1029/2011GL049750.
- Zhao, P., Z. Peng, and K. G. Sabra (2010), Detecting remotely triggered temporal changes around the Parkfield section of the San Andreas fault, *Earthq. Sci.*, **23**(5), 497–509.